THE JOURNAL OF PHYSICAL CHEMISTRY C

Article

pubs.acs.org/JPCC

Bipyridine-Based Nanosized Metal–Organic Framework with Tunable Luminescence by a Postmodification with Eu(III): An Experimental and Theoretical Study

Ying-Ya Liu,[†] Roel Decadt,[‡] Thomas Bogaerts,[†,§] Karen Hemelsoet,[§] Anna M. Kaczmarek,[‡] Dirk Poelman,[∥] Michel Waroquier,[§] Veronique Van Speybroeck,[§] Rik Van Deun,[‡] and Pascal Van Der Voort*[,†]

[†]COMOC—Centre for Ordered Materials, Organometallics and Catalysis, Department of Inorganic and Physical Chemistry, Ghent University, Krijgslaan 281-S3, 9000 Ghent, Belgium

[‡]f-Element Coordination Chemistry Group, Department of Inorganic and Physical Chemistry, Ghent University, Krijgslaan 281-S3, 9000 Ghent, Belgium

[§]Center for Molecular Modeling, Ghent University, Technologiepark 903, 9052 Zwijnaarde, Belgium

[∥]LumiLab, Department of Solid State Sciences, Ghent University, Krijgslaan 281-S1, 9000 Ghent, Belgium

Supporting Information

ABSTRACT: A gallium 2,2′-bipyridine-5,5′-dicarboxylate metal–organic framework, Ga(OH)(bpydc), denoted as COMOC-4 (COMOC = Center for Ordered Materials, Organometallics and Catalysis, Ghent University) has been synthesized via solvothermal synthesis procedure. The structure has the topology of an aluminum 2,2′-bipyridine-5,5′-dicarboxylate − the so-called MOF-253. TEM and SEM micrographs show the COMOC-4 crystals are formed in nanoplates with uniform size of 30–50 nm. The UV–vis spectra of COMOC-4 in methanol solution show maximal electronic absorption at 307 nm. This results from linker to linker transitions as elucidated by time-dependent density functional theory simulations on the linker and COMOC-4 cluster models. When excited at 400 nm, COMOC-4 displays an emission band centered at 542 nm. Upon immersion in different solvents, the emission band for the framework is shifted in the range of 525–548 nm depending on the solvent. After incorporating Eu^{3+} cations, the emission band of the framework is shifted to even shorter wavelengths (505 nm). By varying the excitation wavelengths from 250 to 400 nm, we can fine-tune the emission from red to yellowish green in the CIE diagram. The luminescence behavior of Eu^{3+} cations is well preserved and the solid-state luminescence lifetimes of τ_1 = 45 μs (35.4%) and τ_2 = 162 μs (64.6%) are observed.

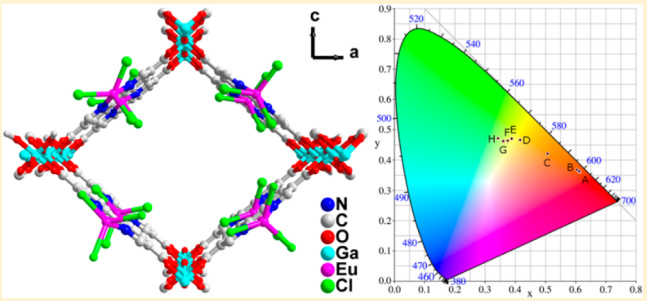

1. INTRODUCTION

Luminescent materials are of great interest and have numerous applications ranging from light emitting devices (LEDs) to materials for medical diagnostics and cell biology. Luminescent metal–organic frameworks (MOFs)[1−4] combining a high, well-defined porosity and an intense fluorescence have gained a lot of attention in the past few years. A recent review article concluded that about 10% of all reported MOFs have interesting luminescence properties.[5] The main advantage of a luminescent MOF is based on the unique inorganic–organic hybrid framework, in which the concentration of the emitting metal ions per unit cell can be systematically adjusted by simply varying the organic linkers. Second, the high surface area and pore volumes make these materials the ideal candidates for sensing.[6,7]

To date, most of the research on synthesizing MOFs has been based on transition metal ions, which have certain coordination motifs, thus allowing a rational synthetic strategy to obtain the desired structures. However, for lanthanide (Ln) MOFs, the research is less extensive, which is obviously due to the higher coordination numbers and the more variable nature of the Ln coordination sphere. This makes a rational design of Ln-based MOFs extremely difficult.[8,9] Thus, to exploit their luminescence properties efficiently, alternative strategies have been explored such as the design or chemical modification of the organic linker to gain ligand emission or alternatively doping the porous MOF materials with a luminescent molecule.[7,10] As Ln-doped materials[11] are widely employed as phosphors for photonic applications such as sensors, solid-state lighting, nonlinear optics, and biomedical analysis, it is obvious that Ln-doped MOFs can pave the way toward novel luminescent materials.

Received: March 2, 2013
Revised: April 24, 2013
Published: April 29, 2013

Furthermore, for luminescence applications, control of the particle size is a powerful strategy to modulate the optical properties, especially for semiconductor nanoparticles.[12−14] This also applies to MOFs and by controlling the synthesis procedure, the crystal size of the MOFs can be downsized to the nanometer scale. These so-called nano-MOFs can provide novel opportunities for catalysis, bioimaging, and sensing.[15−18] For example, Chen et al. reported on Ln-MOFs with Lewis-basic pyridyl sites for sensing of metal ions.[19] Recently, a mixed Ln-MOF has been developed as a luminescent thermometer.[20] However, very few examples of luminescent MOFs have been reported with collaborative functionalities of tunable luminescence and nanoscale processability.[21,22]

To get more detailed information about the geometry and electronic structure of MOFs ab initio calculations can be used. Molecular modeling tools have proven useful in the investigation of electronic structure[23] and spectroscopic properties.[24,25] A theoretical analysis allows us to provide more insight in the molecular structure of the MOF and more specifically the defects and impurities contained in the framework.[26]

Here, we report a new luminescent active gallium-based nano-MOF Ga(OH)(bpydc) ($bpydc^{2-}$ = 2,2′-bipyridine-5,5′-dicarboxylate), denoted as COMOC-4 (COMOC = Center for Ordered Materials, Organometallics and Catalysis, Ghent University). This MOF compound is isostructural to MOF-253, which was recently reported by Yaghi and co-workers.[27] It should be noted that this framework constitutes open 2,2′-bipyridine sites, which is a classical unit for chelating with transition metal or lanthanide ions to form complexes that show intense luminescence.[28−30] By postsynthetic modification, 2,2′-bipyridine sites can bind luminescent Ln^{3+}-ions resulting in luminescent MOFs.[31,32]

2. EXPERIMENTAL AND COMPUTATIONAL SECTION

2.1. Syntheses. The H_2bpydc ligand was prepared according to a published procedure.[33] Methanol used for spectroscopic studies was spectroscopic grade. All other starting materials were commercially available reagents of analytical grade and were used without further purification.

COMOC-4 (Ga(OH)(bpydc)) Synthesis. $Ga(NO_3)_3{\cdot}H_2O$ (0.06 g, 0.22 mmol), H_2Bpydc (0.06 g, 0.25 mmol), and DMF (5 mL) were placed in a 15 mL Pyrex tube and heated at 150 °C for 48 h. This resulted in a green powdered phase in suspension. Upon contact with air, the solid color changed immediately from green to orange. The orange colored gel phase was filtered off, washed consecutively with DMF, methanol and acetone, and dried in vacuum. Afterward, the solid product was suspended in DMF solution (0.5 g per 50 mL DMF), heated at 80 °C for 4 h, filtered off, washed consecutively with DMF and acetone, and dried in vacuum. The yield was 33% based on gallium. IR spectrum (cm^{-1}, KBr pellet): 3379 (br), 1619 (s), 1595 (s), 1421 (s), 1394 (s), 1158 (w), 1050 (w), 847 (w), 775 (m), 705 (w), 600 (w), 479 (w). Calcd for $Ga(OH)(C12H6N2O4){\cdot}2.7H_2O$: C, 38.36; H, 3.27; N, 7.46; Found: C, 38.26; H, 3.12; N, 7.17.

To remove the organic species encapsulated within the pores of the open framework, the sample was activated by Soxhlet extraction in methanol for 24 h at 120 °C and then dried at 120 °C under vacuum overnight. Because of the presence of the −OH group on the gallium building unit, the 1D channels are highly hydrophilic. In ambient air, rehydration occurs. Thus, the activated sample was kept in an inert to prevent possible hydrolysis reactions.

Eu^{3+}@COMOC-4 Preparation. Eu^{3+}@COMOC-4 was prepared by stirring the mixture of 0.05 g of Ga(OH)(bpydc) and 0.033 g $EuCl_3{\cdot}6H_2O$ in 30 mL absolute ethanol at 50 °C for 24 h. The solid was then filtered off, and the yellowish powder was stirred in 15 mL pure ethanol for another 24 h followed by filtration. This procedure was repeated two times to guarantee that all excess $EuCl_3$ salt is removed. IR spectrum (cm^{-1}, KBr pellet): 3370 (br), 2925 (w), 2855 (w), 1616 (s), 1591 (s), 1412 (s), 1384 (s), 1164 (w), 1048 (w), 853 (w), 776 (m), 706 (w), 602 (w), 477 (w). Calcd for $Ga(OH)(C12H6N2O4){\cdot}3H_2O{\cdot}C2H6O{\cdot}0.11EuCl3$: C, 36.76; H, 4.19; N, 6.12; Found: C, 36.82; H, 3.15; N, 5.90.

2.2. Characterization. *X-ray Powder Diffraction Measurements and Thermal Gravimetric Analysis.* X-ray powder diffraction (XRPD) patterns were recorded on a Thermo Scientific ARL X'Tra diffractometer, operated at 40 kV, 40 mA using Cu−Kα radiation (λ = 1.5406 Å). The lattice parameters were determined using the DICVOL program[34] and refined using the STOE's WinXPow[35] software package. Thermal gravimetric analysis (TGA) data were obtained on a Netzsch STA 449 F3 Jupiter-Simultaneous TG-DSC analyzer with a heating rate of 10 °C min^{-1} in air. N_2 sorption measurements were carried on Belsorp II, Bell Japan, Inc. Each sample was activated under vacuum at 120 °C for 3h prior to measurement.

Spectroscopic Characterizations. Fourier transform infrared (FTIR) spectra were recorded in the region of 400−4000 cm^{-1} on a Bruker EQUINOX 55 FTIR spectrometer. The UV−vis absorption spectra were recorded on a PerkinElmer Lambda 950 UV−vis spectrometer in the range of 260−1000 nm. The spectra were recorded using fine suspensions of powder samples (COMOC-4, Eu^{3+}@COMOC-4) with methanol as dispersing solvent. In a typical measurement, 4 mg of powder sample was suspended in 3 mL of methanol in an ultrasonic bath for 5 min. The suspension was transferred to a 10 mm path length quartz cuvette to record the spectra. The diffuse UV−vis reflection spectra (DRS) experiments were carried out using a Varian Cary 500 UV−vis-NIR spectrophotometer with diffuse reflectance accessory (integrated sphere) for spectrophotometric measurements in the range of 200−800 nm. The spectra were converted using the Kubelka−Munk function.

Morphology Characterizations. The particle shape and size was determined using a JEOL JEM2200FS transmission electron microscope with an accelerating voltage of 200 kV. Images were obtained digitally on a Gatan CCD camera. The samples for TEM were prepared on copper grids (size 200 mesh) coated with a carbon support film. 0.01 g of the powder sample was dispersed in 2 mL of methanol and sonificated to prepare the suspension. A drop of the suspension was placed on a copper grid and left to dry in air. Scanning electron microscopy (SEM) images were taken on a FEI Quanta 200FEG microscope with 4 nm resolution operating at 30 kV.

Luminescence Measurements. The photoluminescence measurements were carried out on an Edinburgh Instruments FLSP920 UV−vis-NIR spectrofluorimeter, using a 450 W xenon lamp as the steady-state excitation source and a Hamamatsu R928P PMT detector, which has a response curve between 200 and 900 nm. For time-resolved measurements, the setup uses a 60W pulsed xenon lamp operating at a pulse frequency of 100 Hz.

COMOC-4 sample soaked with various solvents were prepared by immersing the desolvated COMOC-4 in different solvent solution, stirring at room temperature for 0.5 h, filtered, and collecting the solid sample for luminescence measurements.

dx.doi.org/10.1021/jp402154q | J. Phys. Chem. C 2013, 117, 11302−11310

Quantification of Eu Loadings by Means of XRF Analysis. The XRF measurements were performed on Rigaku NexCG, Energy Dispersive X-ray Fluorescence (EDXRF) apparatus. A standard addition method was used using $VO(acac)_2$ as external standard.

2.3. Computational Methodology. All calculations were done with the Gaussian09[36] program. Geometries were optimized using the hybrid B3LYP functional,[37,38] combined with a 6-31+G(d) Pople basis set. UV−vis absorption wavelengths were obtained using a static TD-DFT[39−42] calculation on the optimized geometry using a 6-31+G(d) or a 6-311++G(2df,2p) basis set. Vertical transitions are known to provide good estimates of experimental electronic transitions.[43,44] For the TD-DFT simulations, three DFT functionals have been employed. In order of increasing % HF exchange, we tested HCTH[45] (0% HF exchange), B3LYP[37,38] (20% HF exchange), and CAM-B3LYP[46] (long-range corrected functional with varying amount of HF exchange, up to 63% at large distance). These functionals have already proven successful in the calculation of UV−vis spectra.[24,47] Where applicable, a continuum PCM solvent model for methanol was applied.

For the optimization of the MOF models, clusters were extracted from the crystallographic file of DUT-5,[48] which is similar to COMOC-4; the model was then adapted to correspond with our MOF. In a first step, the carboxyl −OH and −O groups were allowed to relax keeping the rest of the structure fixed. In a second step, these groups were fixed while the rest of the structure was relaxed. This was repeated three times to allow the geometry to fully converge. This procedure is necessary since gallium is significantly bigger then aluminum (from the original crystallographic file) and the bond lengths must be allowed to relax. The fixation of the terminal atoms allows mimicking the rigidity of the crystal in the cluster model. Using this methodology, two clusters were isolated, a smaller one (2 linkers) and a larger one (4 linkers), as shown in Figure 3.

3. RESULTS AND DISCUSSION

The gallium-based nanosized MOF compound has been obtained by mixing gallium(III) nitrate and H_2bpydc (2,2′-bipyridine-5,5′-dicarboxylic acid) in dimethylformamide (DMF) to yield an orange crystalline powder "COMOC-4-as" (as: as-synthesized), $Ga(OH)(bpydc)\cdot 3H_2O$. Afterward, COMOC-4-as was activated by vacuum drying to yield COMOC-4 and this porous structure was postfunctionalized with a solution of europium(III) chloride in ethanol. Both COMOC-4 and Eu^{3+}@COMOC-4 were characterized by powder X-ray diffraction (XRD), thermogravimetric analysis, CHNS elemental analysis, scanning electron microscopy (SEM), transmission electron microscopy (TEM), FTIR spectroscopy, X-ray fluorescence spectroscopy (XRF), UV−vis absorbance, and diffuse reflectance spectroscopy (DRS), as well as steady state and time-resolved luminescence spectroscopy. In addition, the spectroscopic absorbance properties of COMOC-4 are compared with theoretical data using TD-DFT calculations on model clusters representative of the linker as well as of COMOC-4. Electronic transitions are computed using different theoretical methodologies and inspection of the involved molecular orbitals provide insight into the nature of the transitions.

3.1. Structural Characterization. The powder XRD pattern (Figure S1 of the Supporting Information) shows that COMOC-4 is isostructural with DUT-5 (Al(OH)(bpdc)) ($bpdc^{2-}$ = biphenyl-4,4′-dicarboxylate).[48] Laboratory powder XRD data have been used to index the unit cell with orthorhombic unit cell parameters of a = 21.98(24) Å, b = 7.302(8) Å, and c = 17.470(24) Å. The COMOC-4 framework is based on infinite chains of octahedral $GaO_4(OH)_2$ units, where each Ga^{3+} ion is bound to four $bpydc^{2-}$ ligands and two μ_2 trans hydroxide anions. This is a common coordination motif that has already been encountered in a series of M^{3+} carboxylate frameworks (M = Al, Fe, V, Ga, and In).[49,50] The $GaO_4(OH)_2$ chains are aligned parallel to the crystallographic b axis, with the hydroxide and the carboxylate linker alternating on either side of the chains, further linked to each other to form a 3D open framework. After incorporating Eu^{3+} cations into the COMOC-4 framework, the material retained its crystallinity as evidenced by the powder XRD patterns (Figure S1 of the Supporting Information). TEM and SEM images have demonstrated that COMOC-4 crystalline compounds are in the nanosize range consisting of irregularly shaped, crystalline nanoplates with fairly uniform sizes of approximately 30−50 nm. The morphology and size of these nanoparticles does not change upon incorporation of $EuCl_3$ (Figure S2 of the Supporting Information). These crystalline nanoparticle sizes are consistent with the line broadening of the XRD peaks. The representative structure of $EuCl_3$ incorporated on the COMOC-4 framework is depicted in Figure 1. By immersing the COMOC-4 material in a europium-

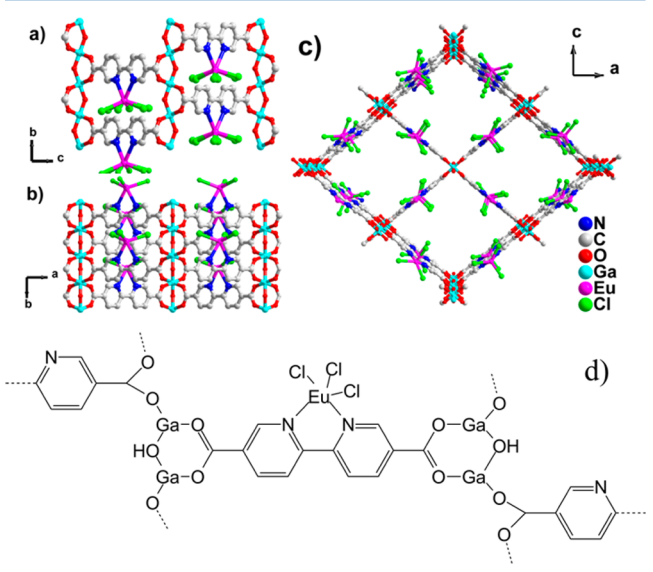

Figure 1. Representative structure of Eu^{3+}@COMOC-4. View perpendicular to (a,b) and along (c) the 1D pore system. The structure model was generated based on the crystal structure of DUT-5.[48] (d) Schematic representation of $EuCl_3$ tethered to the bipyridine site of the MOF by postsynthetic modification.

(III) chloride ethanol solution, 0.38 mmol g^{-1} Eu^{3+} cations were successfully incorporated into the framework affording $Ga(OH)(bpydc)\cdot 0.11EuCl_3$ (referred as Eu^{3+}@COMOC-4 hereafter). The number of europium(III) ions that had been incorporated in the COMOC-4 host has been determined by X-ray fluorescence (XRF) analysis. The XRF result clearly showing that the molar ratio of Eu/Cl is 1/2.993, which in perfect agreement with the incorporation of $EuCl_3$.

The COMOC-4 nanoparticles maintain their permanent microporosity after guest removal, as demonstrated by a type I N_2 sorption isotherm (Figure S3 of the Supporting Information) showing a pore volume of 0.98 cm^3/g, together with BET and Langmuir surface areas of 747 and 918 m^2/g, respectively. After incorporating Eu^{3+} cations, the Eu^{3+}@COMOC-4 shows a

dx.doi.org/10.1021/jp402154q | J. Phys. Chem. C 2013, 117, 11302−11310

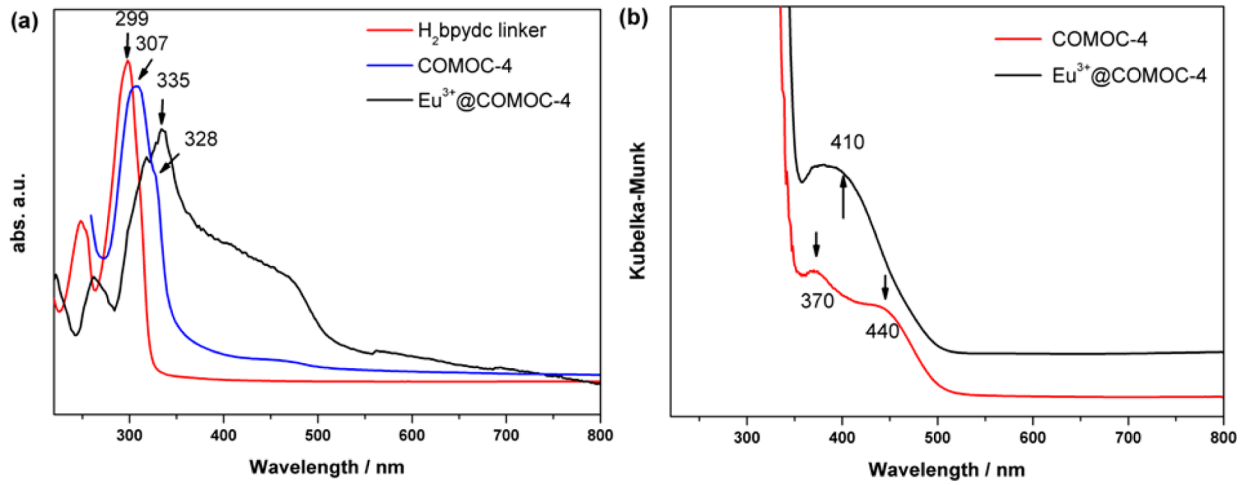

Figure 2. (a) UV−vis absorption spectra of suspended Eu^{3+}@COMOC-4, COMOC-4 in MeOH solution compared to the organic linker dissolved in MeOH solution; (b) solid-state UV−vis spectra calculated from diffuse reflection spectra.

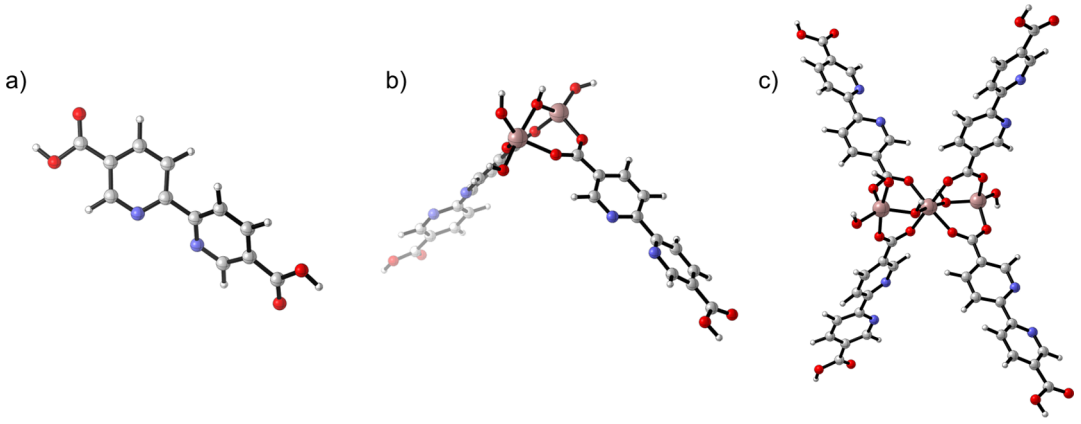

Figure 3. Model for the linker (a) and COMOC-4 (b,c). A small model with two linkers (b) and an extended model with four linkers (c) are investigated.

reduced BET and Langmuir surface area of 493 and 702 $m^2\ g^{-1}$, respectively, and the pore volume reduced to 0.86 cm^3/g. The thermal behavior of COMOC-4 has been examined by means of thermogravimetric analysis (TGA) (Figure S4 of the Supporting Information). The first mass loss in the TGA profiles corresponds to the elimination of solvent in the pores (∼8.5 wt %). The COMOC-4 material is thermally stable up to 300 °C, above which a further weight loss of 62 wt % before 560 °C is indicative of the decomposition of the framework. The final residue (observed, 29.6 wt %; calculated 26.6 wt %) is Ga_2O_3. As for Eu^{3+}@COMOC-4, the incorporation of Eu^{3+} cations does not influence the thermostability of the framework. The TGA curve shows a weight loss consist of 26 wt % of solvent release in the initial stage followed by 50.6 wt % of weight loss due to the framework decomposition. The residue of 24.6 wt % (calculated 24.8%) is Ga_2O_3 and Eu_2O_3. Calculated values are based on the elemental analysis results.

In the FTIR spectra, the absorption bands of the C−O carboxyl bonds attached to the metal centers of the $bpydc^{2-}$ ligand are visible at 1619 and 1595 cm^{-1}, respectively. No free carboxylate species, corresponding to the range 1730−1680 cm^{-1}, is observed (Figure S5 of the Supporting Information).

3.2. UV−vis Absorption Spectra. The UV−vis absorption spectra have been recorded using fine suspensions of powdered samples with methanol as dispersing solvent.

As shown in part a of Figure 2, the H_2bpydc ligand displays one strong absorption band in the UV spectral region centered at 299 nm arising from a $\pi-\pi^*$ transition in the aromatic rings. When coordinated to gallium ions, the absorption spectrum shows a significant red-shift by approximately 8 nm. This progressive red shift is due to the coordination process, which depopulates the electronic aromatic ring of the ligand increasing the HOMO energy and thus decreasing the HOMO−LUMO gap of the coordination compound with respect to the free ligand. Furthermore, the absorption band of COMOC-4 also shows a shoulder at 328 nm and a weak absorption at 440 nm. The Eu^{3+}@COMOC-4 shows only one broad band centered at 335 nm. DRS measurements have also been performed on powdered samples in order to get better resolution in the visible region. As shown in part b of Figure 2, COMOC-4 gives two distinguishable absorption bands at 370 and 440 nm, whereas after incorporation of Eu^{3+} cations these two bands have been replaced by a broader absorption band at around 410 nm.

Ab initio calculations have been used to aid the interpretation of the experimental UV−vis absorption spectra. The H_2bpydc linker is shown in part a of Figure 3. A scan was performed to investigate the geometrical stability of the isolated linker and its influence on the excitation energy. The central dihedral angle N−C−C−N (φ) was varied over 360° during the scan. Results are displayed in Figure 4. It is shown that the isolated linker

dx.doi.org/10.1021/jp402154q | J. Phys. Chem. C 2013, 117, 11302−11310

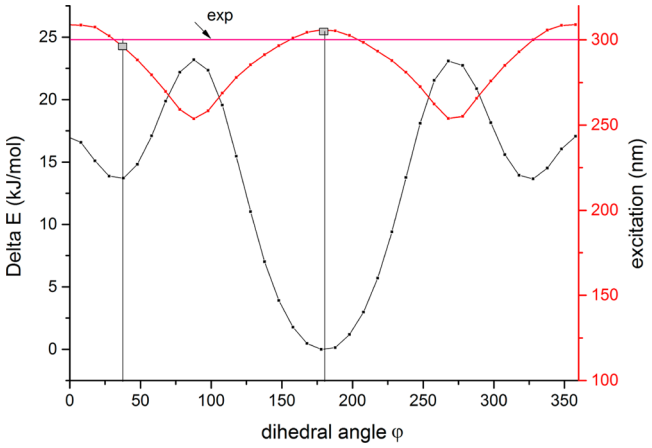

Figure 4. Potential energy in function of the dihedral angle φ (=N−C−C−N) relative to the absolute minimum at φ = 180° (both nitrogens facing away from each other) (black curve and left *y* axis). Also given is the vertical excitation energy at maximum absorbance (red curve and right *y* axis). The B3LYP/6-31+G(d) level of theory with a PCM solvent model for methanol was used. Experimental value of 299 nm is given for reference.

preferentially forms a planar structure with both nitrogen atoms facing away from each other (φ = 180°). The corresponding vertical excitation wavelength with maximal absorbance (computed using B3LYP/6-31+G(d) TD-DFT) of this optimized geometry equals 305 nm without and 316 nm with PCM (polarizable continuum model), respectively. A second minimum (Figure 4) corresponds to a slightly twisted linker structure (φ = 37°), which is only 14 kJ/mol higher in energy compared to the absolute minimum. The absorbance for this model is centered at 288 nm without and at 295 nm with the PCM model. The excitation energy fluctuates significantly in the whole range of the dihedral angle, but at the two minima of the potential energy the B3LYP predictions are quite close to the experimental value justifying the choice of the B3LYP functional. For the sake of completeness, we also performed vertical TD-DFT calculations using other levels of theory. The results are given in Table S1 of the Supporting Information. The main excitation always corresponds to a π–π^* transition, predominantly a HOMO to LUMO transition. The other functionals or extended basis set do not perform better. An interesting feature in Figure 4 is that the experimental value of 299 nm is also fairly well reproduced at the local minimum when both nitrogen atoms are pointing toward each other. This position is ideal to allow interactions with metal ions, such as the Eu^{3+} ions as studied in this work.

For the interpretation of the COMOC-4 spectrum representative cluster models as shown in parts b and c of Figure 3 are used. Two clusters were isolated, containing 2 and 4 linkers, respectively.

Using the smaller cluster and including a PCM model for methanol, the main absorption is found at 310 nm, which is in excellent agreement with the band at 307 nm found experimentally for COMOC-4 in methanol suspension (part a of Figure 2). However, the shoulder at 328 nm is not present in the theoretical spectrum. To explain this second absorption band, different defects were introduced in the model (Figure S6 of the Supporting Information): a dimethyl formamide (DMF) molecule remaining in the pores, excess gallium nitrate on the bipyridine moiety or a cation due to a missing linker or bridging −OH group. In the smaller model, the missing linker was represented by removing a saturating −OH group instead of removing a whole linker since this would make the structure less representative of the real crystal structure. This means that there is no distinction between the two cases. The first two options do not significantly change the position of the main absorption band (Figure S7 of the Supporting Information). The cationic model however, red shifts the main band to 326 nm (Figure 5), in

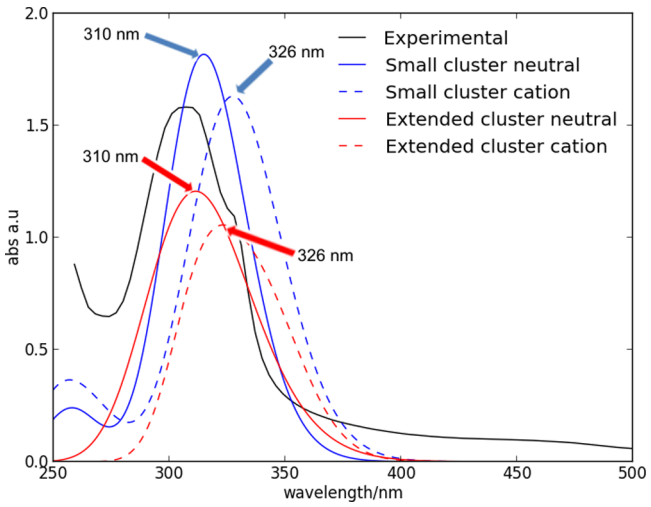

Figure 5. Comparison between the experimental (in black) and calculated (in blue and red) UV−vis spectra for the measurement in suspension using different models for COMOC-4. Results for the neutral models correspond to the full curves, whereas the cationic defect (due to a missing −OH bridge) correspond to the dashed lines. TD-DFT computations were performed using B3LYP/6-31+G(d) including a methanol PCM solvent model.

agreement with experiment. This suggests that the COMOC-4 structure contains cationic defects. To further investigate the nature of this defect, a bigger model containing four linkers was also investigated. The results are also included in Figure 5 and Table S2 of the Supporting Information. With this extended cluster, removing a linker does not remove all features of the crystal structure, hence the different possibilities for a cationic defect could be considered separate. TD-DFT calculations on the extended cluster show an absorption band around 310 nm, which confirms the results of the smaller cluster. Introducing a missing linker defect causes a red-shift toward 321 nm. The missing −OH bridge leads to a main absorption band at 326 nm. The shoulder in the experimental spectrum is thus probably due to the latter defect. These types of cations can occur anywhere in the structure but they are more likely to appear at the surface of a crystal.

The maximal absorption band corresponds with a HOMO−LUMO transition and consists primarily of π–π^* excitations of the linker. This conclusion is manifested in the 3D representation of the HOMO and LUMO orbitals depicted in Figure 6. The coordination of the linker to the metal shifts the excitation to a higher wavelength. The same effect was reported for MOF-5 where the electronic excitations were attributed to the terephthalic acid linker.[25] These observations justify our choice for the B3LYP functional. It is known that CAM-B3LYP performs better when charge transfer is present,[51,52] and this is apparently not the case for our systems.

3.3. Luminescence Properties. It is known that, due to the porous structure, some fluorescent MOF materials are sensitive to the presence or absence of guest solvent molecules and can be used as chemical sensors.[53−58] The luminescence properties of

dx.doi.org/10.1021/jp402154q | J. Phys. Chem. C 2013, 117, 11302−11310

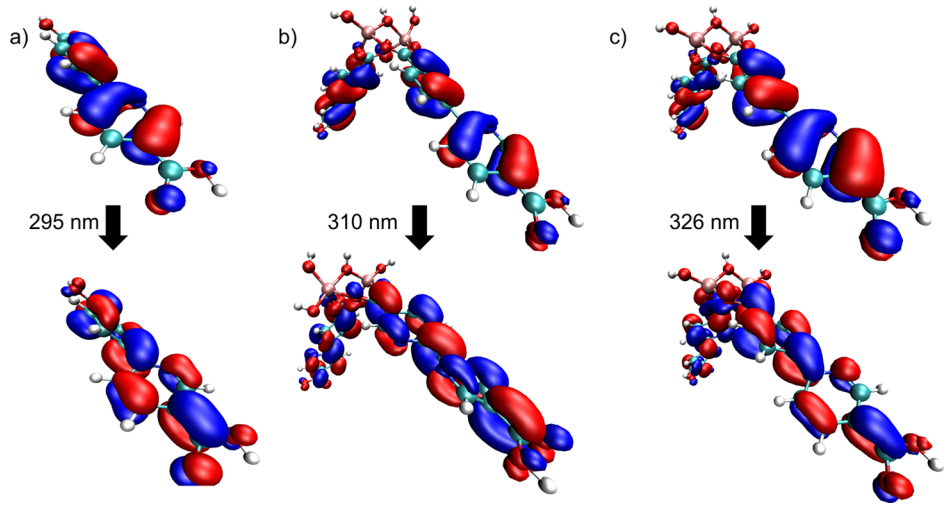

Figure 6. HOMO–LUMO orbitals of the linker (a) the neutral model (b) and the cationic model (c) involved in the $\pi-\pi^*$ transitions exhibiting maximal absorbance.

COMOC-4 have been investigated in the solid state at room temperature. The data are summarized in Table 1 and the emission spectra are displayed in part a of Figure 7. A strong emission band at 526 nm emerges in COMOC-4 when excited at 400 nm. The influences of different solvents on the fluorescence properties of COMOC-4 have been investigated in the solid state at room temperature (Figure 8). With the excitation wavelength fixed at 400 nm, the fluorescence of hydrated COMOC-4 displays a strong emission band at 542 nm. Upon immersing in different solvents, the emission band for the framework is shifted in the range of 525–548 nm indicating a guest-responsive fluorescence property (Figure 8). Note that the free H_2bpydc ligand shows emission in the solid state with three bands centered at 433, 485, and 552 nm,[59] respectively. The blue shift

Table 1. Luminescence Data of COMOC-4, Eu3+@COMOC-4, and H2bpydc

compound	excitation maximum (nm)	emission maximum (nm)	$\tau1/\mu s$	$\tau2/\mu s$
COMOC-4[a]	400	526		
Eu^{3+}@COMOC-4[a]	400	505, 579, 591, 612, 650, 699		
	330	579, 591, 612, 650, 699	45(35.4%)	162(64.6%)
H_2bpydc[b]	390	433, 485, 552		

[a]Soaked with methanol guest molecules. [b]From literature data.[59]

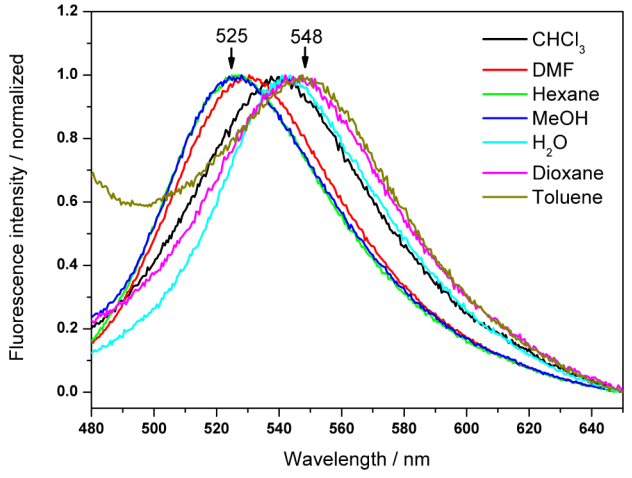

Figure 8. Room temperature solid-state emission spectra of COMOC-4 with different solvent molecules, λ_{exc} = 400 nm, λ_{em} = 525–548 nm.

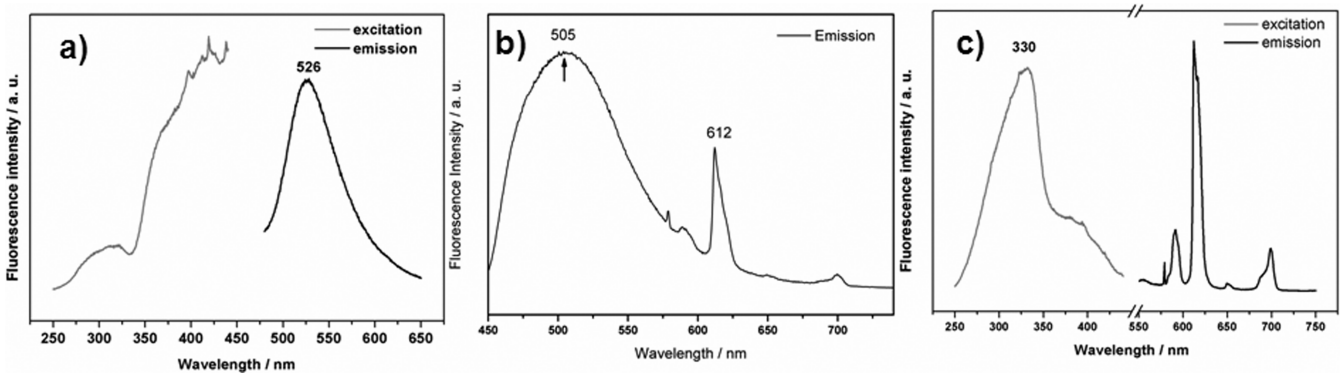

Figure 7. (a) Room temperature solid-state emission and excitation spectra of COMOC-4, λ_{exc} = 400 nm, λ_{em} = 526 nm; (b) room temperature solid-state emission spectra of Eu^{3+}@COMOC-4, λ_{exc} = 400 nm; (c) luminescence spectra of Eu^{3+}@COMOC-4 in the solid state at room temperature, λ_{exc} = 330 nm, λ_{em} = 612 nm.

dx.doi.org/10.1021/jp402154q | J. Phys. Chem. C 2013, 117, 11302–11310

of the emission band of COMOC-4 compound compared to the free organic ligand might be attributed to the ligand-to-metal Ga(III) center charge transfer (LMCT) process.

After incorperating Eu^{3+} cations, the emission band of the framework is shifted to shorter wavelength (505 nm), as shown in part b of Figure 7. In addition, the typical narrow-band emission of Eu^{3+} cations emerges (612 nm), indicating the presence of the Eu^{3+} cations inside the COMOC-4 framework. Part c of Figure 7 further illustrates the solid-state excitation and emission spectra of Eu^{3+}@COMOC-4 excited at 330 nm. When excited at that wavelength, the characteristic sharp emission bands corresponding to the encapsulated Eu^{3+} cations can be clearly observed. The emission spectrum shows peaks at 579, 591, 612, 650, and 699 nm corresponding to the $^5D_0 \rightarrow {}^7F_J$ (J = 0−4) transitions of the Eu^{3+} ion. The fact that the emission band at 612 nm, which corresponds to the hypersensitive $^5D_0 \rightarrow {}^7F_2$ transition, has a high intensity, indicates that the Eu^{3+} ions are not in an inversion center, but are most likely at a site with low symmetry. This is confirmed by the presence of the $^5D_0 \rightarrow {}^7F_0$ transition, located at 579 nm (Figure S8 of the Supporting Information) as this peak should only occur when the Eu^{3+} site symmetry is low. In addition, it appears that only one unique crystallographic Eu^{3+} site is present in the material, because of the fact that the $^5D_0 \rightarrow {}^7F_0$ transition only shows one peak in the emission spectrum (Figure S8 of the Supporting Information). As this is a transition between two nondegenerate states, only one peak can occur. If more than one peak would be seen, this would point to at least two different Eu^{3+} crystal sites. The luminescence decay profile shows a biexponential behavior yielding lifetime values of $\tau_1 = 45\ \mu s$ and $\tau_2 = 162\ \mu s$ (Figure S9 of the Supporting Information).

As both the parent structure and the incorporated Eu^{3+} ions contribute to the compound's luminescence properties, a fine-tuning of the emitted color emission can be easily achieved by adjusting the excitation wavelength. As depicted in Figure 9, by varying the excitation wavelengths from 250 to 400 nm, the CIE (Commission Internationale de l'Eclairage) diagram shows a tunable chromaticity of visible emission from red to yellowish green.

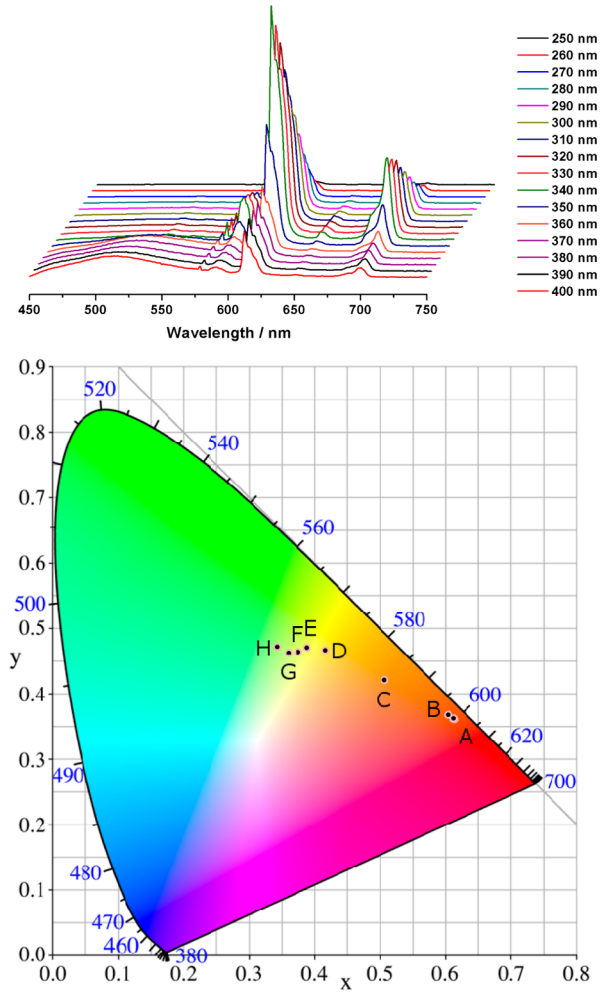

Figure 9. Steady-state emission spectra of Eu^{3+}@COMOC-4 at different exication wavelengths (top). Emission spectra of Eu^{3+}@COMOC-4 plotted on a CIE diagram with excitation wavelengths varying from 250 nm (A) and from 340 to 400 nm (B ∼ H, step size 10 nm) showing tunable chromaticity of visual emission image (bottom).

4. CONCLUSIONS

In summary, a gallium 2,2′-bipyridine-5,5′-dicarboxylate nano-MOF (COMOC-4) has been synthesized and fully characterized. Crystalline nanoplates are obtained with fairly uniform sizes of approximately 30−50 nm. The UV−vis spectra of COMOC-4 in methanol solution show maximal electronic absorption at 307 nm due to linker to linker transitions as elucidated by time-dependent DFT simulations on the linker and COMOC-4 cluster models. TD-DFT simulations on models containing a cationic defect due to a missing −OH group cause absorption at 328 nm. The porous framework displays luminescence mainly due to ligand emission but also shows a clear guest-responsive fluorescence property. Moreover, when COMOC-4 framework is further functionalized with Eu^{3+} cations, excitation of the Eu^{3+}@COMOC-4 at 330 nm results in bright red luminescence originating from the Eu^{3+} cations and thus enhanced the overall luminescence of the resulting material. As both the parent structure and the incorporated Eu^{3+} ions contribute to the luminescence properties, a fine-tuning of the emission color can be easily achieved by adjusting the excitation wavelength. The present work provides a convenient and effective route for tuning luminescent properties via a postsynthetic functionalization process.

■ ASSOCIATED CONTENT

Ⓢ Supporting Information

Powder XRD, TEM, and SEM micrographs, N_2 sorption/desorption isotherms, TGA, FTIR spectrum, and additional information concerning theoretical calculations. This material is available free of charge via the Internet at http://pubs.acs.org.

■ AUTHOR INFORMATION

Corresponding Author

*Tel: +32-9-264.44.42, e-mail: pascal.vandervoort@ugent.be.

Notes

The authors declare no competing financial interest.

■ ACKNOWLEDGMENTS

The authors acknowledge the financial support from the Ghent University BOF Grant (Nr. 01P02911T, 01N01010) and GOA Grant (01G00710); the Hercules Foundation (project AUGE/09/024 "Advanced Luminescence Setup"); the Research Foundation-Flanders (FWO-Vlaanderen, project G.0081.10N); BELSPO in the frame of IAP 6/27 and the European Research Council (FP7(2007-2013) ERC Grant (Nr. 240483). Computa-

tional resources and services provided by Ghent University are greatly acknowledged.

REFERENCES

(1) Park, Y. K.; Choi, S. B.; Kim, H.; Kim, K.; Won, B.-H.; Choi, K.; Choi, J.-S.; Ahn, W.-S.; Won, N.; Kim, S.; et al. Crystal Structure and Guest Uptake of a Mesoporous Metal−Organic Framework Containing Cages of 3.9 and 4.7 nm in Diameter. *Angew. Chem., Int. Ed.* **2007**, *46*, 8230−8233.

(2) Cui, Y.; Xu, H.; Yue, Y.; Guo, Z.; Yu, J.; Chen, Z.; Gao, J.; Yang, Y.; Qian, G.; Chen, B. A Luminescent Mixed-Lanthanide Metal-Organic Framework Thermometer. *J. Am. Chem. Soc.* **2012**, *134*, 3979−3982.

(3) Xiao, Y.; Cui, Y.; Zheng, Q.; Xiang, S.; Qian, G.; Chen, B. A Microporous Luminescent Metal-Organic Framework for Highly Selective and Sensitive Sensing of Cu(2+) in Aqueous Solution. *Chem. Commun.* **2010**, *46*, 5503−5505.

(4) Takashima, Y.; Martinez Martinez, V.; Furukawa, S.; Kondo, M.; Shimomura, S.; Uehara, H.; Nakahama, M.; Sugimoto, K.; Kitagawa, S. Molecular Decoding Using Luminescence from an Entangled Porous Framework. *Nat. Commun.* **2011**, 2.

(5) Cui, Y.; Yue, Y.; Qian, G.; Chen, B. Luminescent Functional Metal-Organic Frameworks. *Chem. Rev.* **2012**, *112*, 1126−1162.

(6) Rieter, W. J.; Taylor, K. M. L.; Lin, W. B. Surface Modification and Functionalization of Nanoscale Metal-Organic Frameworks for Controlled Release and Luminescence Sensing. *J. Am. Chem. Soc.* **2007**, *129*, 9852−9853.

(7) Buso, D.; Jasieniak, J.; Lay, M. D. H.; Schiavuta, P.; Scopece, P.; Laird, J.; Amenitsch, H.; Hill, A. J.; Falcaro, P. Highly Luminescent Metal-Organic Frameworks through Quantum Dot Doping. *Small* **2012**, *8*, 80−88.

(8) Decadt, R.; Van Hecke, K.; Depla, D.; Leus, K.; Weinberger, D.; Van Driessche, I.; Van Der Voort, P.; Van Deun, R. Synthesis, Crystal Structures, and Luminescence Properties of Carboxylate Based Rare-Earth Coordination Polymers. *Inorg. Chem.* **2012**, *51*, 11623−11634.

(9) Ji, M.; Lan, X.; Han, Z. P.; Hao, C.; Qiu, J. S. Luminescent Properties of Metal-Organic Framework Mof-5: Relativistic Time-Dependent Density Functional Theory Investigations. *Inorg. Chem.* **2012**, *51*, 12389−12394.

(10) An, J.; Shade, C. M.; Chengelis-Czegan, D. A.; Petoud, S.; Rosi, N. L. Zinc-Adeninate Metal-Organic Framework for Aqueous Encapsulation and Sensitization of Near-Infrared and Visible Emitting Lanthanide Cations. *J. Am. Chem. Soc.* **2011**, *133*, 1220−1223.

(11) Wang, G. F.; Peng, Q.; Li, Y. D. Lanthanide-Doped Nanocrystals: Synthesis, Optical-Magnetic Properties, and Applications. *Acc. Chem. Res.* **2011**, *44*, 322−332.

(12) Lee, J.; Govorov, A. O.; Dulka, J.; Kotov, N. A. Bioconjugates of Cdte Nanowires and Au Nanoparticles: Plasmon-Exciton Interactions, Luminescence Enhancement, and Collective Effects. *Nano Lett.* **2004**, *4*, 2323−2330.

(13) Zheng, J.; Ding, Y.; Tian, B. Z.; Wang, Z. L.; Zhuang, X. W. Luminescent and Raman Active Silver Nanoparticles with Polycrystalline Structure. *J. Am. Chem. Soc.* **2008**, *130*, 10472−+.

(14) Maldiney, T.; Sraiki, G.; Viana, B.; Gourier, D.; Richard, C.; Scherman, D.; Bessodes, M.; Van den Eeckhout, K.; Poelman, D.; Smet, P. F. In Vivo Optical Imaging with Rare Earth Doped $Ca_2Si_5N_8$ Persistent Luminescence Nanoparticles. *Opt. Mater. Express* **2012**, *2*, 261−268.

(15) Horcajada, P.; Chalati, T.; Serre, C.; Gillet, B.; Sebrie, C.; Baati, T.; Eubank, J. F.; Heurtaux, D.; Clayette, P.; Kreuz, C.; et al. Porous Metal-Organic-Framework Nanoscale Carriers as a Potential Platform for Drug Delivery and Imaging. *Nat. Mater.* **2010**, *9*, 172−178.

(16) Lin, W. B.; Rieter, W. J.; Taylor, K. M. L. Modular Synthesis of Functional Nanoscale Coordination Polymers. *Angew. Chem., Int. Ed.* **2009**, *48*, 650−658.

(17) Wee, L. H.; Lohe, M. R.; Janssens, N.; Kaskel, S.; Martens, J. A. Fine Tuning of the Metal-Organic Framework $Cu_3(BTC)_2$ HKUST-1 Crystal Size in the 100 Nm to 5 Micron Range. *J. Mater. Chem.* **2012**, *22*, 13742−13746.

(18) Aguado, S.; Canivet, J.; Farrusseng, D. Engineering Structured MOF at Nano and Macroscales for Catalysis and Separation. *J. Mater. Chem.* **2011**, *21*, 7582−7588.

(19) Chen, B. L.; Wang, L. B.; Xiao, Y. Q.; Fronczek, F. R.; Xue, M.; Cui, Y. J.; Qian, G. D. A Luminescent Metal-Organic Framework with Lewis Basic Pyridyl Sites for the Sensing of Metal Ions. *Angew. Chem., Int. Ed.* **2009**, *48*, 500−503.

(20) Cui, Y. J.; Xu, H.; Yue, Y. F.; Guo, Z. Y.; Yu, J. C.; Chen, Z. X.; Gao, J. K.; Yang, Y.; Qian, G. D.; Chen, B. L. A Luminescent Mixed-Lanthanide Metal-Organic Framework Thermometer. *J. Am. Chem. Soc.* **2012**, *134*, 3979−3982.

(21) Liu, K.; You, H. P.; Zheng, Y. H.; Jia, G.; Song, Y. H.; Huang, Y. J.; Yang, M.; Jia, J. J.; Guo, N.; Zhang, H. J. Facile and Rapid Fabrication of Metal-Organic Framework Nanobelts and Color-Tunable Photoluminescence Properties. *J. Mater. Chem.* **2010**, *20*, 3272−3279.

(22) Xu, H.; Rao, X. T.; Gao, J. K.; Yu, J. C.; Wang, Z. Q.; Dou, Z. S.; Cui, Y. J.; Yang, Y.; Chen, B. L.; Qian, G. D. A Luminescent Nanoscale Metal-Organic Framework with Controllable Morphologies for Spore Detection. *Chem. Commun.* **2012**, *48*, 7377−7379.

(23) Fuentes-Cabrera, M.; Nicholson, D. M.; Sumpter, B. G.; Widom, M. Electronic Structure and Properties of Isoreticular Metal-Organic Frameworks: The Case of M-Irmof1 (M = Zn, Cd, Be, Mg, and Ca). *J. Chem. Phys.* **2005**, *123*, 124713−124715.

(24) Huang, Y.; Liu, T.; Lin, J.; Lue, J.; Lin, Z.; Cao, R. Homochiral Nickel Coordination Polymers Based on Salen(Ni) Metalloligands: Synthesis, Structure, and Catalytic Alkene Epoxidation. *Inorg. Chem.* **2011**, *50*, 2191−2198.

(25) Ji, M.; Lan, X.; Han, Z.; Hao, C.; Qiu, J. Luminescent Properties of Metal−Organic Framework MOF-5: Relativistic Time-Dependent Density Functional Theory Investigations. *Inorg. Chem.* **2012**, *51*, 12389−12394.

(26) Vermoortele, F.; Vandichel, M.; Van de Voorde, B.; Ameloot, R.; Waroquier, M.; Van Speybroeck, V.; De Vos, D. E. Electronic Effects of Linker Substitution on Lewis Acid Catalysis with Metal-Organic Frameworks. *Angew. Chem., Int. Ed.* **2012**, *51*, 4887−4890.

(27) Bloch, E. D.; Britt, D.; Lee, C.; Doonan, C. J.; Uribe-Romo, F. J.; Furukawa, H.; Long, J. R.; Yaghi, O. M. Metal Insertion in a Microporous Metal-Organic Framework Lined with 2,2′-Bipyridine. *J. Am. Chem. Soc.* **2010**, *132*, 14382−14384.

(28) Ziessel, R.; Maestri, M.; Prodi, L.; Balzani, V.; Vandorsselaer, A. Dinuclear Eu3+, Tb3+, and Gd3+ Complexes of a Branched Hexaazacyclooctadecane Ligand Containing 6 2,2′-Bipyridine Pendant Units. *Inorg. Chem.* **1993**, *32*, 1237−1241.

(29) Puntus, L. N.; Lyssenko, K. A.; Pekareva, I. S.; Bunzli, J. C. G. Intermolecular Interactions as Actors in Energy-Transfer Processes in Lanthanide Complexes with 2,2′-Bipyridine. *J. Phys. Chem. B* **2009**, *113*, 9265−9277.

(30) Bhasikuttan, A. C.; Suzuki, M.; Nakashima, S.; Okada, T. Ultrafast Fluorescence Detection in Tris(2,2 ′-Bipyridine)Ruthenium(II) Complex in Solution: Relaxation Dynamics Involving Higher Excited States. *J. Am. Chem. Soc.* **2002**, *124*, 8398−8405.

(31) Prodi, L.; Maestri, M.; Ziessel, R.; Balzani, V. Luminescent Eu-3+, Tb-3+, and Gd-3+ Complexes of a Branched-Triazacyclononane Ligand Containing 3 2,2′-Bipyridine Units. *Inorg. Chem.* **1991**, *30*, 3798−3802.

(32) Bekiari, V.; Pistolis, G.; Lianos, P. Intensely Luminescent Materials Obtained by Combining Lanthanide Ions, 2,2 ′-Bipyridine, and Poly(Ethylene Glycol) in Various Fluid or Solid Environments. *Chem. Mater.* **1999**, *11*, 3189−3195.

(33) Szeto, K. C.; Kongshaug, K. O.; Jakobsen, S.; Tilset, M.; Lillerud, K. P. Design, Synthesis and Characterization of a Pt-Gd Metal-Organic Framework Containing Potentially Catalytically Active Sites. *Dalton Trans.* **2008**, 2054−2060.

(34) Boultif, A.; Louer, D. Indexing of Powder Diffraction Patterns for Low-Symmetry Lattices by the Successive Dichotomy Method. *J. Appl. Crystallogr.* **1991**, *24*, 987−993.

(35) STOE WinXPOW version 2.11, Stoe & Cie GmbH, Darmstadt, Germany, 2005.

(36) Frisch, M. J.; G. W., T., Schlegel, H. B.; Scuseria, G. E.; Robb, M. A.; Cheeseman, J. R.; Scalmani, G.; Barone, V.; Mennucci, B.; Petersson,

G. A., et al. *Gaussian 09*, Revision A.02; Gaussian, Inc.: Wallingford CT; 2009.
(37) Becke, A. D. Density-Functional Thermochemistry. 3. The Role of Exact Exchange. *J. Chem. Phys.* **1993**, *98*, 5648−5652.
(38) Lee, C. T.; Yang, W. T.; Parr, R. G. Development of the Colle-Salvetti Correlation-Energy Formula into a Functional of the Electron-Density. *Phys. Rev. B* **1988**, *37*, 785−789.
(39) Bauernschmitt, R.; Ahlrichs, R. Treatment of Electronic Excitations within the Adiabatic Approximation of Time Dependent Density Functional Theory. *Chem. Phys. Lett.* **1996**, *256*, 454−464.
(40) Runge, E.; Gross, E. K. U. Density-Functional Theory for Time-Dependent Systems. *Phys. Rev. Lett.* **1984**, *52*, 997−1000.
(41) Stratmann, R. E.; Scuseria, G. E.; Frisch, M. J. An Efficient Implementation of Time-Dependent Density-Functional Theory for the Calculation of Excitation Energies of Large Molecules. *J. Chem. Phys.* **1998**, *109*, 8218−8224.
(42) Dreuw, A.; Head-Gordon, M. Single-Reference Ab Initio Methods for the Calculation of Excited States of Large Molecules. *Chem. Rev.* **2005**, *105*, 4009−4037.
(43) Gonzalez, L.; Escudero, D.; Serrano-Andres, L. Progress and Challenges in the Calculation of Electronic Excited States. *ChemPhysChem* **2012**, *13*, 28−51.
(44) Adamo, C.; Jacquemin, D. The Calculations of Excited-State Properties with Time-Dependent Density Functional Theory. *Chem. Soc. Rev.* **2013**, *42*, 845−856.
(45) Boese, A. D.; Handy, N. C. A New Parametrization of Exchange−Correlation Generalized Gradient Approximation Functionals. *J. Chem. Phys.* **2001**, *114*, 5497−5503.
(46) Yanai, T.; Tew, D. P.; Handy, N. C. A New Hybrid Exchange−Correlation Functional Using the Coulomb-Attenuating Method (CAM-B3LYP). *Chem. Phys. Lett.* **2004**, *393*, 51−57.
(47) De Meyer, T.; Hemelsoet, K.; Van der Schueren, L.; Pauwels, E.; De Clerck, K.; Van Speybroeck, V. Investigating the Halochromic Properties of Azo Dyes in an Aqueous Environment by Using a Combined Experimental and Theoretical Approach. *Chem.—Eur. J.* **2012**, *18*, 8120−8129.
(48) Senkovska, I.; Hoffmann, F.; Froba, M.; Getzschmann, J.; Bohlmann, W.; Kaskel, S. New Highly Porous Aluminium Based Metal-Organic Frameworks: Al(OH)(ndc) (ndc = 2,6-Naphthalene Dicarboxylate) and Al(OH)(bpdc) (bpdc = 4,4 ′-Biphenyl Dicarboxylate). *Microporous Mesoporous Mater.* **2009**, *122*, 93−98.
(49) Loiseau, T.; Serre, C.; Huguenard, C.; Fink, G.; Taulelle, F.; Henry, M.; Bataille, T.; Ferey, G. A Rationale for the Large Breathing of the Porous Aluminum Terephthalate (MIL-53) Upon Hydration. *Chem.—Eur. J.* **2004**, *10*, 1373−1382.
(50) Jacobson, A. J.; Vougo-Zanda, M.; Huang, J.; Anokhina, E.; Wang, X. Q. Tossing and Turning: Guests in the Flexible Frameworks of Metal(III) Dicarboxylates. *Inorg. Chem.* **2008**, *47*, 11535−11542.
(51) Jacquemin, D.; Planchat, A.; Adamo, C.; Mennucci, B. TD-DFT Assessment of Functionals for Optical 0−0 Transitions in Solvated Dyes. *J. Chem. Theory Comput.* **2012**, *8*, 2359−2372.
(52) Peach, M. J. G.; Tozer, D. J. Overcoming Low Orbital Overlap and Triplet Instability Problems in TDDFT. *J. Phys. Chem. A* **2012**, *116*, 9783−9789.
(53) Chen, B.; Yang, Y.; Zapata, F.; Lin, G.; Qian, G.; Lobkovsky, E. B. Luminescent Open Metal Sites within a Metal-Organic Framework for Sensing Small Molecules. *Adv. Mater.* **2007**, *19*, 1693−+.
(54) Wang, F.; Yu, R.; Zhang, Q.-S.; Zhao, Z.-G.; Wu, X.-Y.; Xie, Y.-M.; Qin, L.; Chen, S.-C.; Lu, C.-Z. Solvent-Dependent Luminescent Cu(I) Framework Based on 5-(4-Pyridyl)Tetrazole. *J. Solid State Chem.* **2009**, *182*, 2555−2559.
(55) Wang, C.; Lin, W. B. Diffusion-Controlled Luminescence Quenching in Metal-Organic Frameworks. *J. Am. Chem. Soc.* **2011**, *133*, 4232−4235.
(56) Bauer, C. A.; Timofeeva, T. V.; Settersten, T. B.; Patterson, B. D.; Liu, V. H.; Simmons, B. A.; Allendorf, M. D. Influence of Connectivity and Porosity on Ligand-Based Luminescence in Zinc Metal-Organic Frameworks. *J. Am. Chem. Soc.* **2007**, *129*, 7136−7144.
(57) Feng, P. L.; Leong, K.; Allendorf, M. D. Charge-Transfer Guest Interactions in Luminescent Mofs: Implications for Solid-State Temperature and Environmental Sensing. *Dalton Trans.* **2012**, *41*, 8869−8877.
(58) Stylianou, K. C.; Heck, R.; Chong, S. Y.; Bacsa, J.; Jones, J. T. A.; Khimyak, Y. Z.; Bradshaw, D.; Rosseinsky, M. J. A Guest-Responsive Fluorescent 3d Microporous Metal-Organic Framework Derived from a Long-Lifetime Pyrene Core. *J. Am. Chem. Soc.* **2010**, *132*, 4119−4130.
(59) Zhao, J. W.; Shi, D. Y.; Cheng, H. L.; Chen, L. J.; Ma, P. T.; Niu, J. Y. One-Pot Syntheses, Structures and Properties of Two Novel 1-D Copper Complexes: $[Cu_2(II)(hbpdc)_2Cl_2]_2{\cdot}2H_2O$ and $Cu{-}1(H_2bpdc)Cl$ (H_2bpdc = 2,2′-Bipyridyl-5,5′-Dicarboxylic Acid). *Inorg. Chem. Commun.* **2010**, *13*, 822−827.